Electronic Supplementary Information (ESI)

A Dual-Locked Triarylamine Donor Enables High-Performance Deep-red/NIR Thermally Activated Delayed Fluorescence Organic Light-Emitting Diodes

Hui Wang,[a] Jia-Xiong Chen,[b] Lu Zhou,[a] Xi Zhang,[a] Jia Yu,[a] Kai Wang,[ac]* and Xiao-Hong Zhang[ad]*

[a] Institute of Functional Nano & Soft Materials (FUNSOM), Soochow University, Suzhou, Jiangsu 215123, P. R. China

[b] School of Chemical Engineering and Light Industry, Guangdong University of Technology, Guangzhou, Guangdong, 510006, P.R. China

[c] Jiangsu Key Laboratory for Carbon-Based Functional Materials & Devices, Soochow University, Suzhou, 215123, Jiangsu, PR China

[d] Jiangsu Key Laboratory of Advanced Negative Carbon Technologies, Soochow University, Suzhou, 215123, Jiangsu, PR China

Corresponding Author

wkai@suda.edu.cn, xiaohong_zhang@suda.edu.cn

General Information

1. Materials. All commercially available reagents were used as received unless otherwise stated. All reactions were carried out using Schlenk techniques under a nitrogen atmosphere. ^{1}H and ^{13}C NMR spectra were measured on a Bruker 400 MHz spectrometer with tetramethylsilane (TMS) as the internal standard. Mass analyses were recorded by an Autoflex MALDI-TOF mass spectrometer.

2. Theoretical calculation. The optimized structures, distributions of HOMO and LUMO, excited state levels and natural transition orbitals (NTOs) of the lowest adiabatic excited states were analyzed by the B3LYP/6-31 g (d) basis set via a multifunctional wavefunction analyzer (Multiwfn 3.6)[1].

3. Thermal and electrochemical measurements. Thermogravimetric analysis (TGA) was performed on a TA SDT 2960 instrument at a heating rate of 10 ˚C min^{-1} under nitrogen. The temperature at 5% weight loss was used as the decomposition temperature (T_d). Differential scanning calorimetry (DSC) was performed on a TA DSC 2010 unit at a heating rate of 10 ˚C min^{-1} under nitrogen. Cyclic voltammetry was performed on a CHI 660 instrument. Individual samples were dissolved in dichloromethane solution and degassed with nitrogen gas for 15 minutes before the test. 0.1 M tetrabutylammonium perchlorate in 10^{-3} M dichloromethane solution served as the supporting electrolyte with ferrocene/ferrocenium (Fc/Fc+) as the internal reference.

4. Measurement of absorption and emission characteristics. UV–Vis absorption spectra were recorded on a Hitachi U-3900 spectrophotometer. PL spectra were recorded on a Hitachi F-4600 fluorescence spectrophotometer with default collection intervals. Transient fluorescence decays were measured with a Quantaurus-Tau fluorescence lifetime spectrometer (C11367-32, Hamamatsu Photonics) with an excitation wavelength of 373 nm and pulse width of 100 ps. The absolute PL quantum yields were recorded on a Hamamatsu Quantaurus-QY quantum yield spectrometer (C13534-11).

5. Single-Crystal Structure. Diffraction data were collected on a Rigaku R-AXIS-RAPID diffractometer using ω-scan mode with graphite-monochromator MoKα radiation. The structure determination was solved with direct methods using the SHELXTL programs and refined with full-matrix least squares on F^2. All crystallographic information in CIF format has been deposited at the Cambridge Crystallographic Center (CCDC) under deposition number 2226280 for DCN-DLB via www.ccdc.cam.ac.uk/data_request/cif.

6. Device fabrication and measurement of EL characteristics. OLEDs were fabricated on indium tin oxide (ITO)-coated transparent glass substrates. The ITO conductive layer has a thickness of ca. 100 nm and a sheet resistance of ca. 30 Ω per square. The substrates were cleaned sequentially with ethanol, acetone, and deionized water, dried in an oven, and finally exposed to UV ozone for 15 min. All organic materials and metal layers were thermally evaporated under a vacuum of ca. 10^{-5} Torr. Four identical OLED devices, each with a 0.1 cm^2 area, were formed on an ITO glass substrate.

Synthetic procedure and characterization

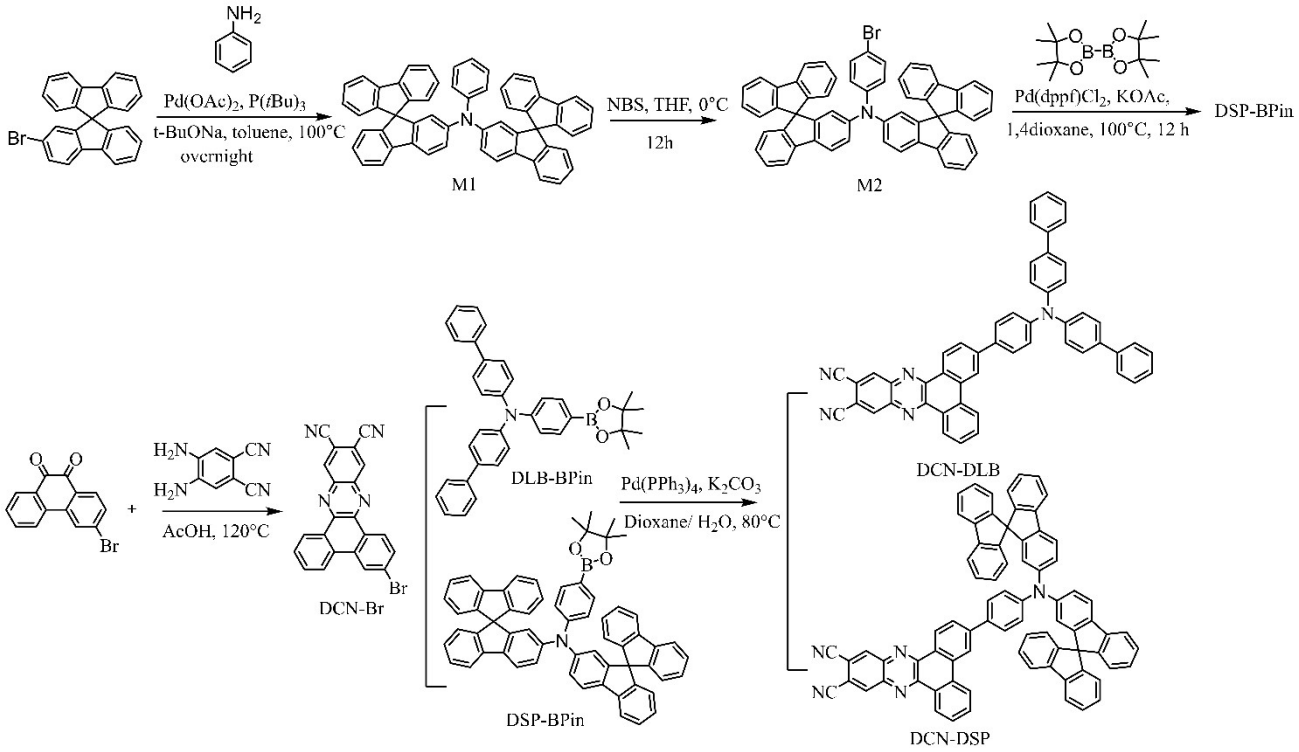

Scheme S1. Experimental procedures of DCN-DLB and DCN-DSP.

Synthesis of N-(9,9'-spirobi[fluoren]-2-yl)-N-phenyl-9,9'-spirobi[fluoren]-2-amine (M1).

A mixture of 2-bromo-9,9'-spirobifluorene (4.4 g, 11.0 mmol), phenylamine (465 mg, 5.0 mmol), $Pd(OAc)_2$ (301 mg, 0.30 mmol), P(*t*-Bu)$_3$ (296 mg, 0.10 mmol), *t*-BuONa (1.9 g, 20.0 mmol) and 120 mL toluene were added to a 250 mL flask and stirred at 100 °C overnight under N_2 atmosphere. After reaction completed, the solution was cooled to room temperature, and extracted with brine and dichloromethane. After removal of the solvent, the residue was purified by column chromatography and white solid was gained (3.6 g, 4.8 mmol). Yield: 96%. ^{1}H (400 MHz, $CDCl_3$, δ) 7.72 (dd, J = 15.5, 7.6 Hz, 6H), 7.59 (d, J = 8.3 Hz, 2H), 7.35-7.29 (m, 6H), 7.10 (t, J = 7.5 Hz, 4H), 7.02 (t, J = 7.4 Hz, 2H), 6.94-6.87 (m, 4H), 6.72 (dd, J = 16.8, 7.6 Hz, 7H), 6.63 (d, J = 7.5 Hz, 2H), 6.45 (d, J = 1.9 Hz, 2H). MALDI-TOF MS (mass m/z): 721.48 [M]+; calculated for $C_{56}H_{35}N$ 721.28.

Synthesis of N-(9,9'-spirobi[fluoren]-2-yl)-N-(4-bromophenyl)-9,9'-spirobi[fluoren]-2-amine (M2). A mixture of M1 (2.9 g, 4 mmol), N-Bromosuccinimide (783 mg, 4.4 mmol) and 150 mL THF were added to a 250 mL flask at 0 °C for 4h and then stirred at room temperature for 8 h. After reaction completed, the solution was concentrated and purified by column chromatography with PE and DCM

(10/1, v/v) as eluent solvents to gain white solid (2.32g). Yield: 58%. ^{1}H (400 MHz, $CDCl_3$, δ) 7.99 (s, 1H), 7.73 (dd, J = 20.7, 7.6 Hz, 6H), 7.59 (d, J = 8.2 Hz, 2H), 7.32 (t, J = 7.4 Hz, 5H), 7.09 (t, J = 7.2 Hz, 4H), 7.02 (t, J = 7.4 Hz, 2H), 6.96 (d, J = 8.9 Hz, 2H), 6.89 (dd, J = 8.2, 2.0 Hz, 2H), 6.72 (d, J = 7.6 Hz, 4H), 6.62 (d, J = 7.6 Hz, 2H), 6.55 (d, J = 8.9 Hz, 2H), 6.42 (d, J = 2.0 Hz, 2H). MALDI-TOF MS (mass m/z): 801.24 [M]+; calculated for $C_{56}H_{34}BrN$ 801.19

Synthesis of N-(9,9'-spirobi[fluoren]-2-yl)-N-(4-(4,4,5,5-tetramethyl-1,3,2-dioxaborolan-2-yl)phenyl)-9,9'-spirobi[fluoren]-2-amine (DSP-BPin).

A mixture of M2 (1.6 g, 2.0 mmol), Bis(pinacolato)diboron (755.0 mg, 3.0 mmol), $Pd(dppf)Cl_2$ (73.2 mg, 0.10 mmol), KOAc (6.1 g, 6.0 mmol), with 100 mL 1,4-dioxane were added to a 250 mL flask and stirred at 100 °C for 12 h. After reaction completed, the solution was cooled to room temperature, extracted with brine and dichloromethane and dried over anhydrous Na_2SO_4. The obtained crude product was further purified by column chromatography with PE and DCM (8/1, v/v) as eluent solvents to obtain white solid (1.1 g, 1.36 mmol). Yield: 68%. ^{1}H (400 MHz, $CDCl_3$, δ) 8.03 (s, 3H), 7.74 (dd, J = 14.0, 7.6 Hz, 6H), 7.62 (d, J = 8.2 Hz, 2H), 7.35-7.31 (m, 5H), 7.11 (t, J = 7.5 Hz, 4H), 7.06-7.02 (m, 2H), 6.95-6.91 (m, 2H), 6.74 (d, J = 7.7 Hz, 4H), 6.65 (dd, J = 13.8, 8.0 Hz, 4H), 6.50 (dd, J = 9.9, 1.9 Hz, 2H), 1.24 (s, 12H). MALDI-TOF MS (mass m/z): 847.48 [M]+; calculated for $C_{62}H_{46}BNO_2$ 847.36.

Synthesis of 3-bromodibenzo[a,c]phenazine-11,12-dicarbonitrile (DCN-Br). A mixture of 3-bromophenanthrene-9,10-dione (1.72 g, 6 mmol) and 4,5-diaminophthalonitrile (0.95 g, 6 mmol) in acetic acid (40 mL) was heated to reflux for 12 hours. After cooling to room temperature, the resulting mixture was poured into water (100 mL) and then filtered. The solid was washed with water and methanol several times. The crude product was reprecipitated from chloroform/methanol to give the target material as a yellow solid in 90% yield (2.21 g). ^{1}H (600 MHz, $CDCl_3$, δ) 9.37 (d, J = 8.2 Hz, 1H), 9.22 (d, J = 6.9 Hz, 1H), 8.82 (d, J = 7.9 Hz, 2H), 8.72 (s, 1H), 8.52 (d, J = 10.4 Hz, 1H), 7.94-7.90 (m, 2H), 7.87-7.80 (m, 1H). MALDI-TOF MS (mass m/z): 408.0 [M]+; calculated for $C_{22}H_9BrN_4$ 408.1.

Synthesis of 3-(4-(di([1,1'-biphenyl]-4-yl)amino)phenyl)dibenzo[a,c]phenazine-11,12-dicarbonitrile (DCN-DLB). A mixture of DCN-Br (816 mg, 2 mmol) and DLB-Bpin (1.15 g, 2.2 mmol) in 40 ml dioxane and 4 mL aqueous Na_2CO_3 solution (2 M) and $Pd(PPh_3)_4$ (0.12 g, 0.1 mmol) were refluxed under argon for 24 h in a 100 mL round-bottom flask. After cooling to room

temperature, the reaction mixture was extracted with brine and dichloromethane and dried over anhydrous Na_2SO_4. After removal of the solvent, the residue was purified by column chromatography to give a deep red powder (1.1 g, 1.56 mmol). Yield: 78%. ^{1}H (400 MHz, $CDCl_3$, δ) 9.39 (d, J = 8.5 Hz, 2H), 8.79 (d, J = 11.8 Hz, 3H), 8.70 (d, J = 8.2 Hz, 1H), 8.04 (d, J = 9.8 Hz, 1H), 7.95 (t, J = 8.2 Hz, 1H), 7.82 (dd, J = 23.5, 8.1 Hz, 3H), 7.63 (dd, J = 16.8, 8.0 Hz, 8H), 7.48 (t, J = 7.6 Hz, 4H), 7.35 (dd, J = 19.9, 8.6 Hz, 8H). Unfortunately, owing to its poor solubility, its ^{13}C NMR spectra could not be obtained. MALDI-TOF MS (mass m/z): 725.26 [M]+; calculated for $C_{52}H_{31}N_5$ 725.34. Elemental analysis (%) for $C_{52}H_{31}N_5$: C, 86.05, H, 4.30, N, 9.65; found: C, 86.12, H, 4.36, N, 9.58.

Synthesis of 3-(4-(di(9,9'-spirobi[fluoren]-2-yl)amino)phenyl)dibenzo[a,c]phenazine-11,12-dicarbonitrile (DCN-DSP). Using a similar synthesis procedure for DCN-DLB with DSP-Bpin instead of DLB-Bpin (1.3 g, 63%). ^{1}H (400 MHz, $CDCl_3$, δ) 9.31 (dd, J = 29.3, 8.3 Hz, 2H), 8.80-8.52 (m, 4H), 7.93 (t, J = 7.3 Hz, 1H), 7.84-7.75 (m, 8H), 7.69 (d, J = 8.2 Hz, 2H), 7.39-7.33 (m, 8H), 7.15 (t, J = 7.5 Hz, 4H), 7.09-7.02 (m, 4H), 6.87 (d, J = 8.5 Hz, 2H), 6.80 (d, J = 7.6 Hz, 4H), 6.67 (d, J = 7.6 Hz, 2H), 6.58 (s, 2H). Unfortunately, owing to its extremely poor solubility, its ^{13}C NMR spectra could not be obtained. MALDI-TOF MS (mass m/z): 1049.35 [M]+; calculated for $C_{78}H_{43}N_5$ 1049.48. Elemental analysis (%) for $C_{78}H_{43}N_5$: C, 89.20, H, 4.13, N, 6.67; found: C, 89.24, H, 4.08, N, 6.74.

Thermal and electrochemical properties

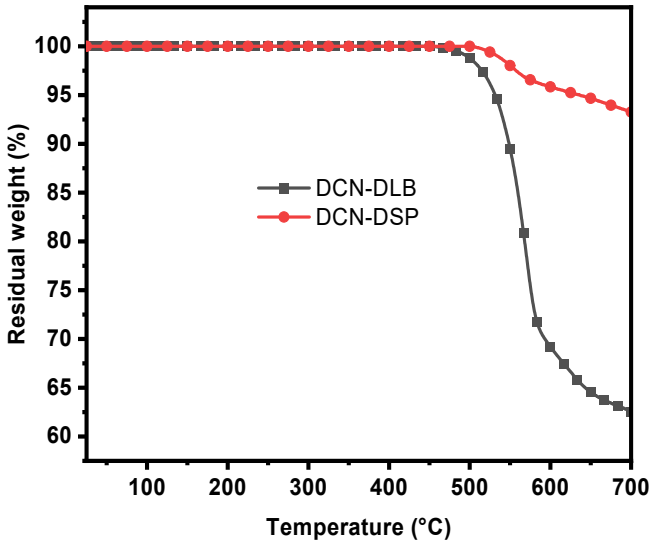

Fig. S1 TGA curves of DCN-DLB and DCN-DSP.

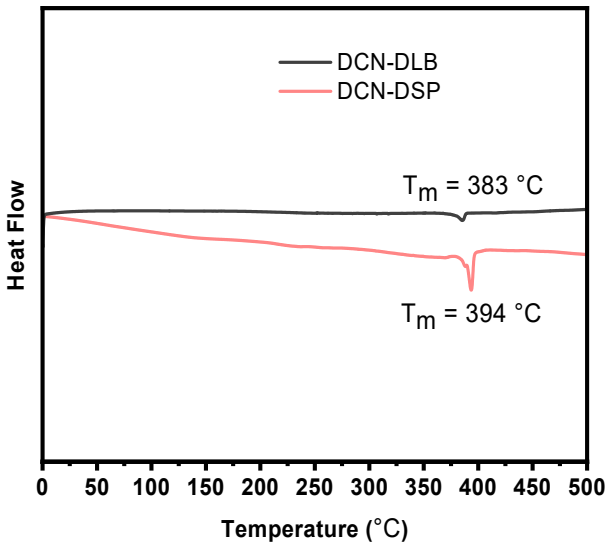

Fig. S2 DSC curves of DCN-DLB and DCN-DSP.

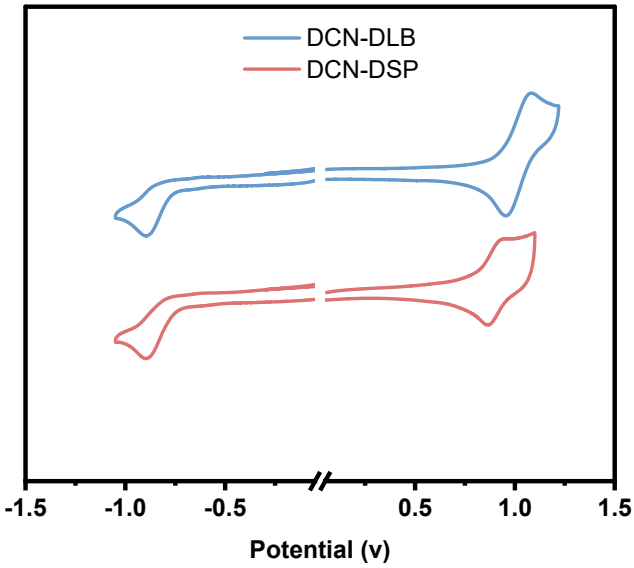

Fig. S3 Cyclic voltammogram curves of DCN-DLB and DCN-DSP.

Theoretical calculations

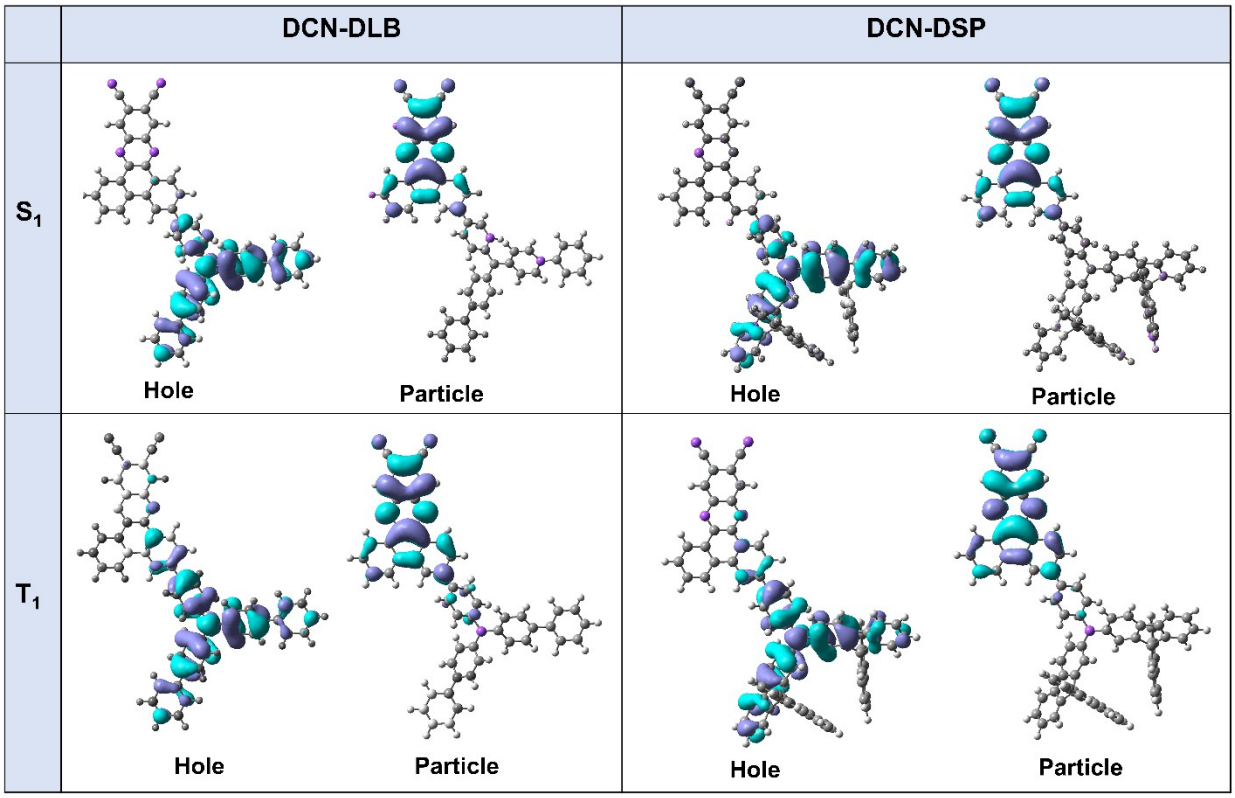

Fig. S4 Natural transition orbital (NTO) analysis of DCN-DLB and DCN-DSP.

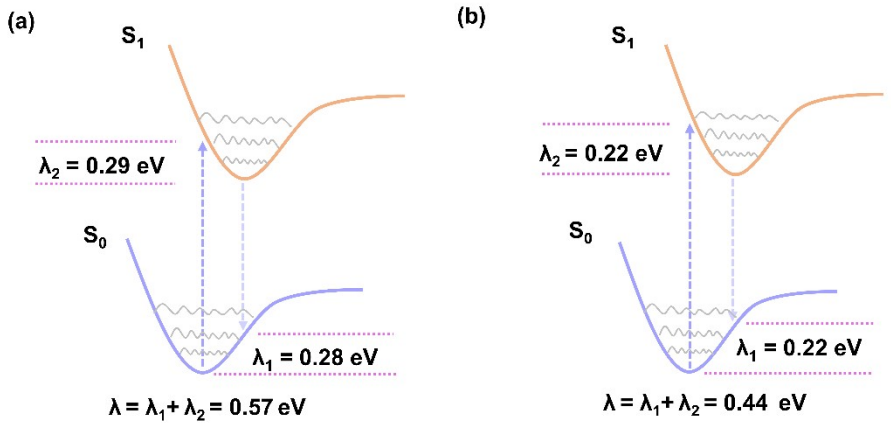

Fig. S5 Reorganization energy (λ) analysis of DCN-DLB and DCN-DSP.

Table S1. Summary of the theoretical calculated results of DCN-DLB and DCN-DSP.

Molecule	HOMO	LUMO	S_1	T_1	ΔE_{ST}	f
DCN-DLB	-5.15	-3.01	1.93	1.75	0.18	0.18
DCN-DSP	-5.08	-3.00	1.83	1.69	0.14	0.22

Photophysical properties

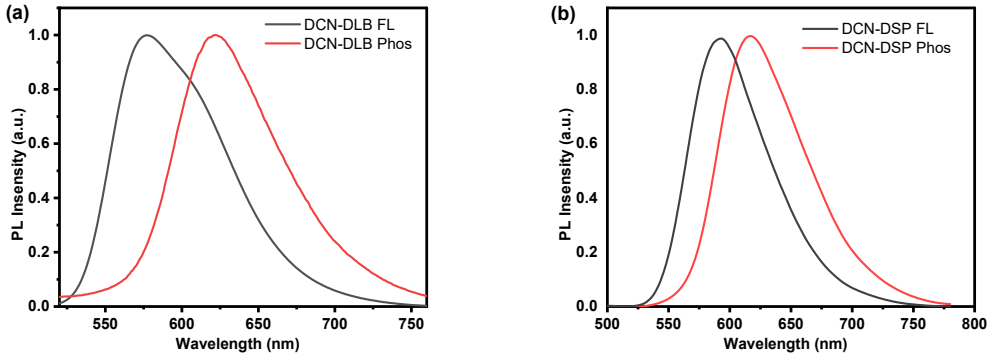

Fig. S6 Normalized fluorescence and phosphorescence spectra of the two compounds at 77 K in toluene.

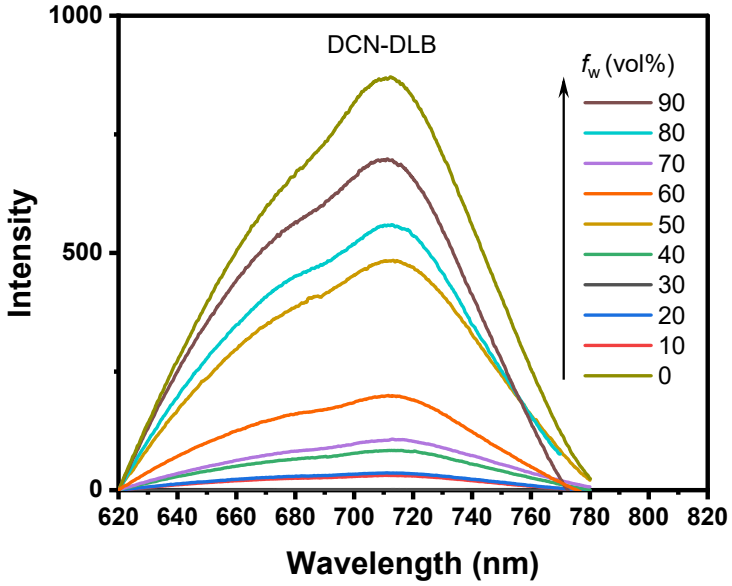

Fig. S7 Fluorescence spectra of DCN-DLB in THF/water solution with increasing water content.

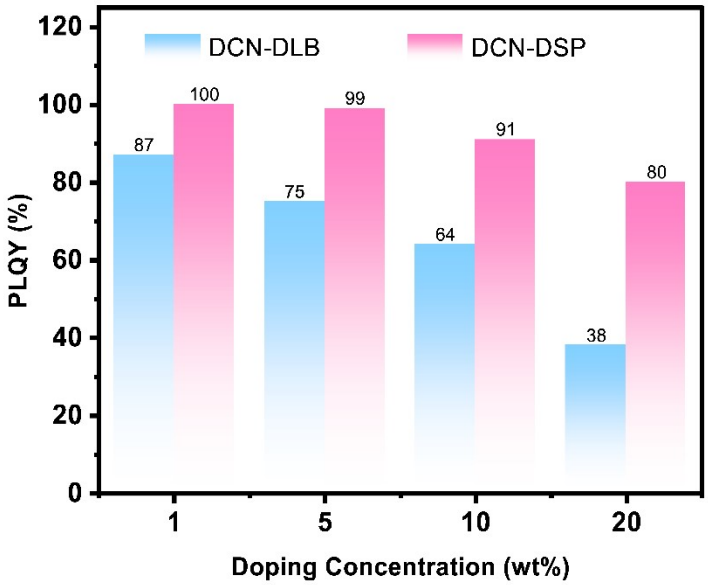

Fig. S8 PLQYs of DCN-DLB and DCN-DSP in CBP-doped films at different concentrations.

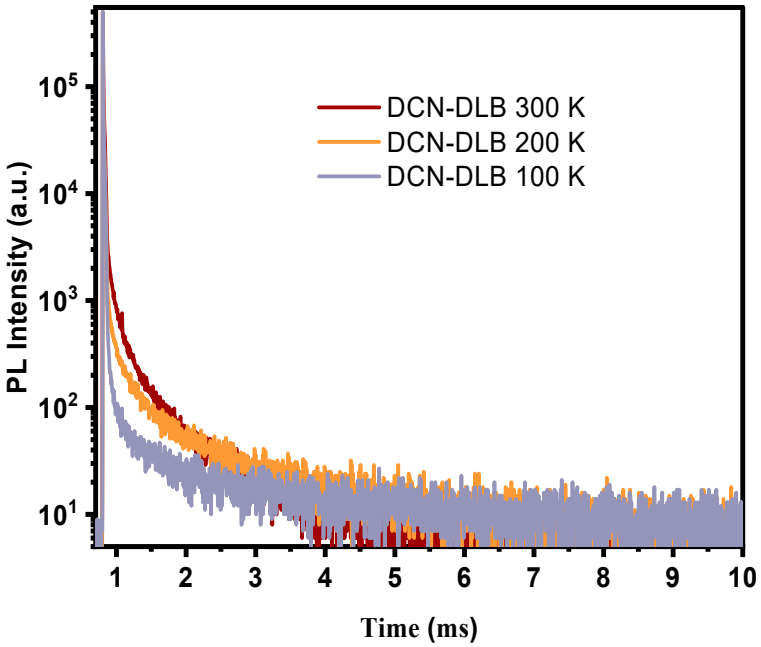

Fig. S9 Transient photoluminescence decay curves of 1 wt% DCN-DLB in CBP thin film under an inert atmosphere at different temperatures.

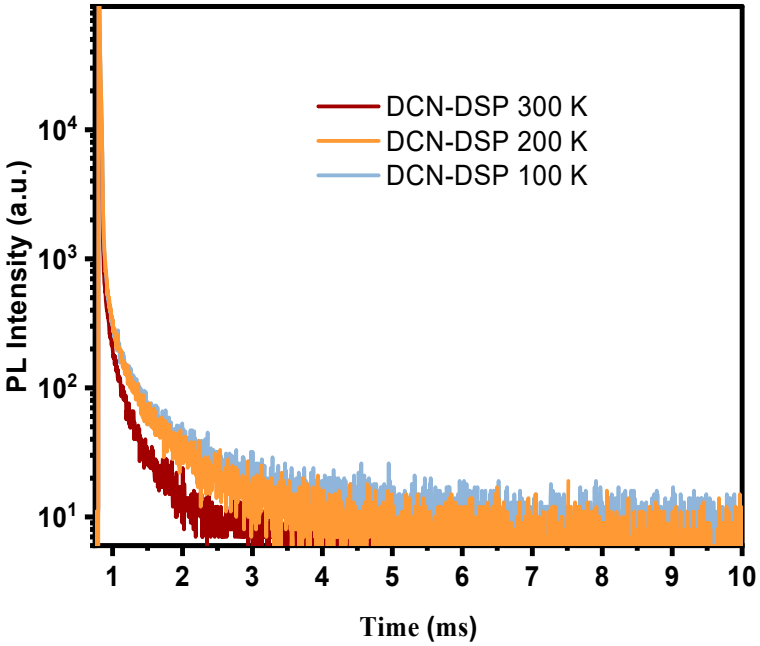

Fig. S10 Transient photoluminescence decay curves of 5 wt% DCN-DSP in CBP thin film under an inert atmosphere at different temperatures.

Determination of Rate Constants

The quantum efficiencies and rate constants were determined using the following equations:

$$k_p = \frac{1}{\tau_p} \quad \text{(S1);}$$

$$k_d = \frac{1}{\tau_d} \quad \text{(S2);}$$

$$k_r^s = k_p \phi_p \quad \text{(S3);}$$

$$k_{ISC} = k_p(1 - \phi_p) \quad \text{(S4)};$$

$$k_{RISC} = \frac{k_p k_d \phi_d}{k_{ISC} \phi_p} \quad \text{(S5)};$$

$$\phi = k_r^s/(k_r^s + k_{IC}^S) \quad \text{(S6)}$$

where τ_p and τ_d represent the prompt and delayed decay lifetimes, respectively; ϕ, ϕ_p and ϕ_d are the total, prompt and delayed fluorescence quantum efficiencies, respectively; and k_p, k_{ISC}, k_{RISC}, and k_d are the rate constants of prompt fluorescence, ISC, RISC, and delayed fluorescence decay, respectively.

The prompt lifetimes were obtained by exponentially fitting of the prompt PL curves with mono-exponential function as, $I_t = I_0 e^{-t/\tau_p}$, in which I is the photoluminescence intensity, t is the decay time, and τ_p is the prompt lifetime, respectively. The experimental PL decays in Figure 3d can be expressed with a biexponential function as, $I_t = B_1 e^{-t/\tau_p} + B_2 e^{-t/\tau_d}$ in which, B_1 and B_2 are the quantities of emission components, τ_p and τ_d are the lifetimes of prompt (p) and delayed (d) components, respectively.

Table S2. Kinetic parameters of DCN-DLB and DCN-DSP.

EMLs	ϕ_{PL}	ϕ_P/ϕ_d	τ_p	τ_d	k_r^s	k_P	k_d	k_{ISC}	k_{RISC}	k_{IC}^S
	[%]	[%]	[ns]	[μs]	[10^7 s^{-1}]	[10^7 s^{-1}]	[10^3 s^{-1}]	[10^7 s^{-1}]	[10^3 s^{-1}]	[10^6 s^{-1}]
DCN-DLB	87	41/46	11.2	511	3.6	8.9	1.9	5.3	3.7	5.4
DCN-DSP	99	46/53	10.7	222	4.3	9.3	4.5	5.1	9.6	0.4

Electroluminescence Properties

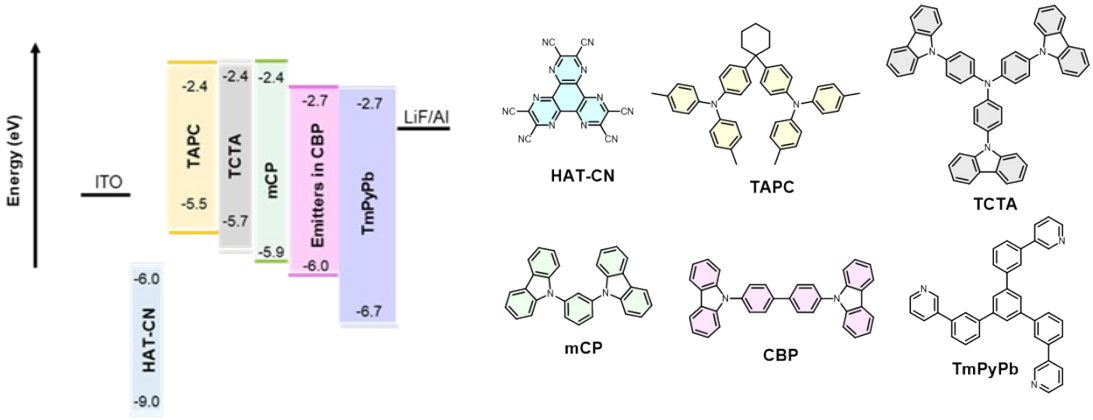

Fig. S11 OLED structures and the corresponding materials used in the devices.

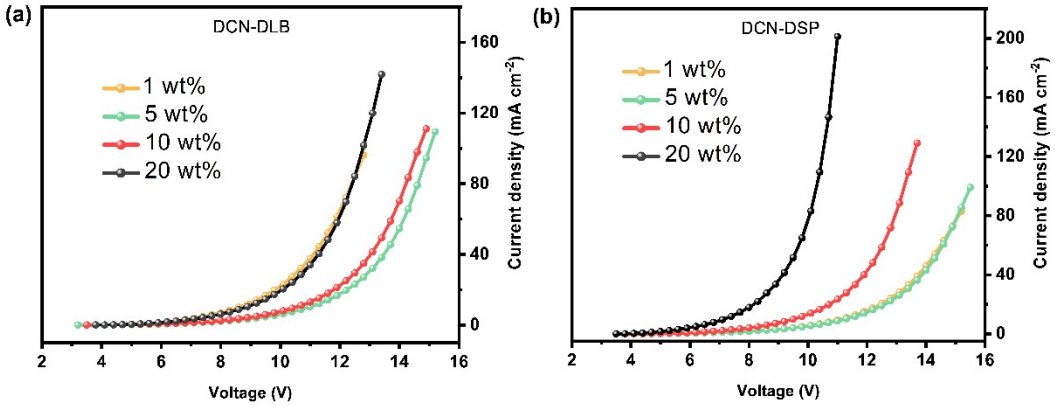

Fig. S12 Current density versus voltage curves based on (a) DCN-DLB and (b) DCN-DSP.

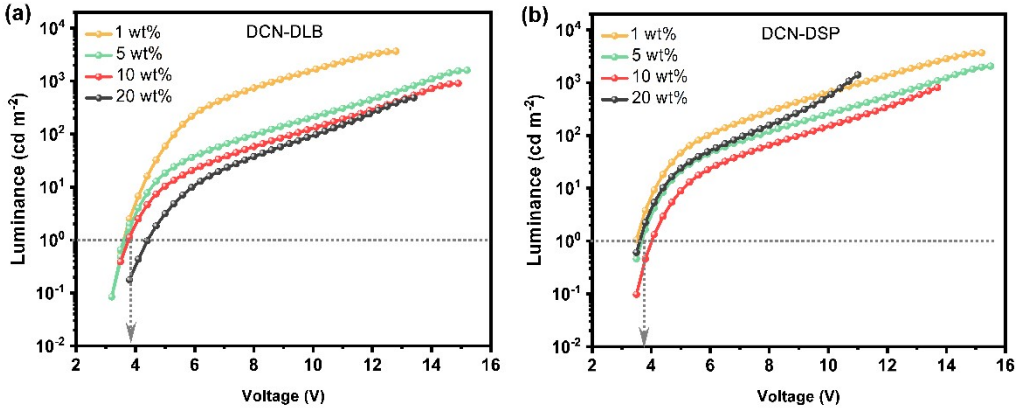

Fig. S13 Luminance versus voltage curves based on (a) DCN-DLB and (b) DCN-DSP.

Table S3. EL performances of the doped devices based on DCN-DLB and DCN-DSP.

EML	Wt (%)	V_{on}[a] (v)	Peak (nm)	CE_{max}/$CE_{@1}$[a]/ $CE_{@100}$[b]/$CE_{@1000}$[c] (cd A^{-1})	PE_{max}/$PE_{@1}$[a]/ $PE_{@100}$[b]/$PE_{@1000}$[c] (lm W^{-1})	EQE_{max}/$EQE_{@1}$[a]/ $EQE_{@100}$[b]/ $EQE_{@1000}$[c] (%)	Roll-off$_{@100}$/ Roll-off$_{@1000}$ (%)	CIE (x, y)
DCN-DLB	1	3.6	612	39.4/38.9/21.5/9.3	35.3/33.9/12.6/3.4	25.2/24.9/13.8/6.0	45.2/76.2	(0.61, 0.39)
	5	3.7	664	11.6/11.5/4.8/2.1	10.4/9.9/1.9/0.5	21.5/21.4/8.8/3.7	59.0/82.8	(0.64, 0.35)
	10	3.8	688	4.1/4.0/1.9/--	3.1/3.4/0.6/--	15.7/15.5/7.1/--	54.8/--	(0.68, 0.31)
	20	4.5	720	0.8/0.8/0.5/--	0.5/0.6/0.2/--	9.8/9.6/5.7/--	41.8/--	(0.70, 0.29)
DCN-DSP	1	3.5	624	48.8/48.8/24.2/9.9	43.8/43.8/12.7/2.8	36.0/36.0/17.7/7.4	50.8/79.4	(0.60, 0.40)
	5	3.7	660	19.8/18.9/7.5/3.0	17.8/16.0/3.1/0.7	36.2/34.6/13.7/5.6	62.1/84.5	(0.65, 0.34)
	10	3.9	676	8.1/8.2/2.7/1.4	7.3/6.4/1.1/0.3	26.1/24.3/8.7/4.5	66.7/82.7	(0.68, 0.32)
	20	3.7	716	2.1/2.0/1.0/0.7	1.7/1.8/0.4/0.2	21.3/20.7/10.3/7.5	51.6/64.8	(0.70, 0.29)

[a] Turn-on voltage, measured at 1 cd/m^2; [b] Measured at 100 cd/m^2; [c] Measured at 1000 cd/m^2.

Table S4. EL performances of reported representative deep-red TADF OLEDs with EL peaks in the range of 650-676 nm.

Emitters	EL (nm)	CE (cd A^{-1})	PE (lm W^{-1})	EQE (%)	CIE (x, y)	References
DCN-DSP	660	19.8	17.8	36.2	(0.65, 0.34)	This work

	676	8.1	7.3	26.1	(0.68, 0.32)	
DDTPACz-DCPP	652	10.6	8.7	13.1	(0.63, 0.37)	[2]
pTPA-DPPZ	652	8.10	3.63	12.3	(0.67, 0.33)	[3]
BCN-TPA	656	12.9	12.7	27.6	(0.686, 0.304)	[4]
TPA-QCN	656	9.3	10.0	12.8	(0.64, 0.35)	[5]
PIPAQ	656	--	--	2.1	(0.64, 0.36)	[6]
tBuTPA-CNQx	655	7.3	6.4	17.4	(0.63, 0.35)	[7]
	662	5.1	2.9	16.7	(0.67, 0.32)	
*p*CNQ-TPA	660	13.4	13.8	30.3	(0.69, 0.31)	[8]
TPA-PPDCN	664	8.4	8.8	20.2	(0.68, 0.32)	[9]
	676	5.7	5.6	18.8	(0.68, 0.31)	
TPA-DCPP	668	4.0	4.0	9.8	(0.68, 0.32)	[10]
APDC-DTPA	668	--	--	12.3	--	[11]
Da-CNBPz	670	6.2	7.0	15.0	(0.66, 0.34)	[12]
CN-TPA	668	11.75	13.67	22.80	(0.64, 0.33)	[13]
TPA-DQP	676	5.69	4.70	18.3	(0.67, 0.32)	[14]

Table S5. EL performances of reported representative NIR TADF OLEDs with EL peaks in the range of 680-750 nm.

Emitters	EL (nm)	EQE (%)	References
DCN-DSP	716	21.3	This work
CN-TPA	688	18.41	[13]
	698	15.05	
TPA-CN-N4	689	21.0	[15]
APDC-DTPA	693	10.19	[11]
DPA-Ph-DBPzDCN	698	7.68	[16]
TPA-QCN	700	9.4	[5]
	728	3.9	
TPAAP	700	14.1	[17]
T-β-IQD	711	9.44	[18]
Curcuminoid derivative	721	～10	[19]
TBSMCN	728	9.4	[20]
	750	14.25	
TPA-PZTCN	734	13.4	[21]

NMR Spectra

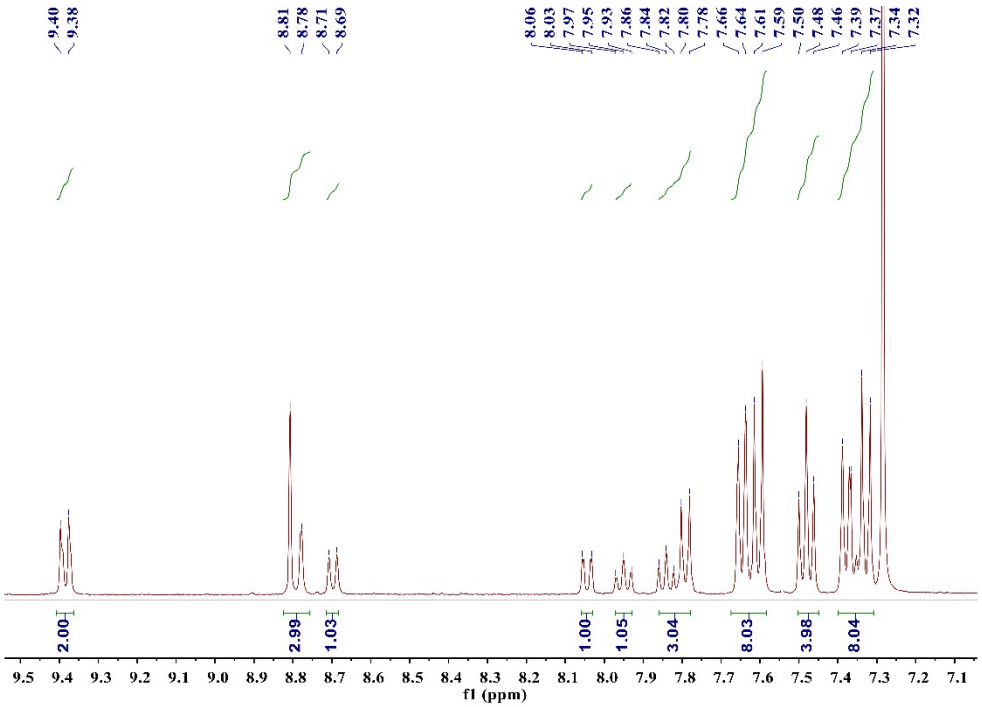

Fig. S14. [1]H NMR spectra of DCN-DLB in chloroform-*d*.

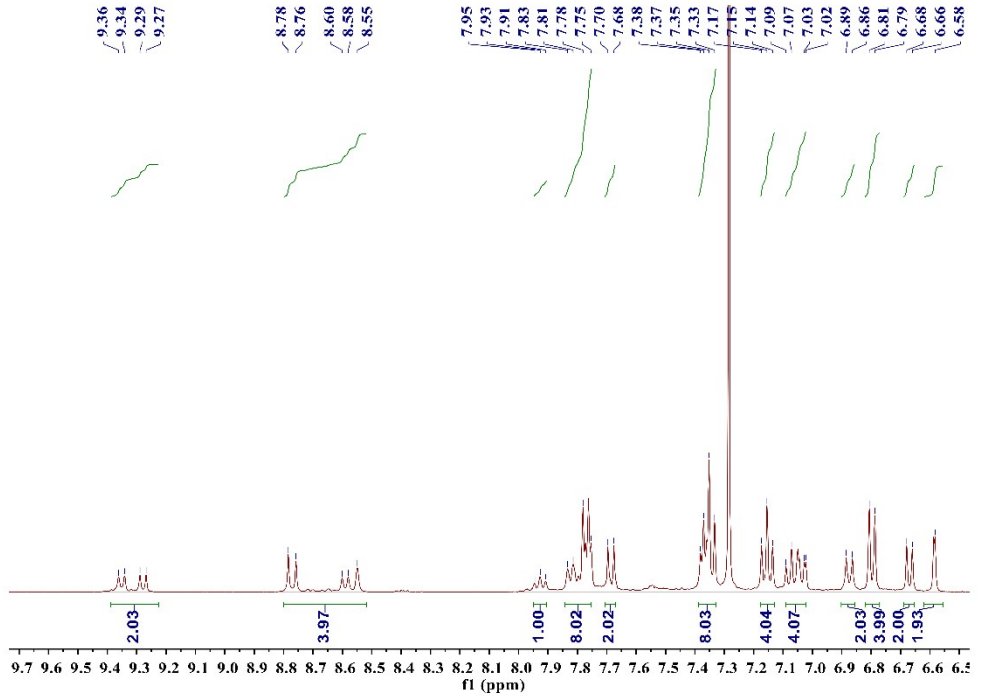

Fig. S15. [1]H NMR spectra of DCN-DSP in chloroform-*d*.

References

1. T. Lu, F. Chen, *J. Comput. Chem.*, 2012, **33**, 580-592.

2. B. Wang, H. Yang, Y. Zhang, G. Xie, H. Ran, T. Wang, Q. Fu, Y. Ren, N. Sun, G. Zhao, J.-Y. Hu, Q. Wang, *J. Mater. Chem. C.*, 2019, **7**, 12321-12327.

3. B. Zhao, H. Wang, C. Han, P. Ma, Z. Li, P. Chang, H. Xu, *Angew. Chem. Int. Ed*., 2020, **59**, 19042-19047.
4. H. Wang, J. X. Chen, X. C. Fan, Y. C. Cheng, L. Zhou, X. Zhang, J. Yu, K. Wang, X. H. Zhang, *ACS. Appl. Mater. Interfaces*., 2023, **15**, 1685.
5. C. Li, R. Duan, B. Liang, G. Han, S. Wang, K. Ye, Y. Liu, Y. Yi, Y. Wang, *Angew. Chem. Int. Ed*., 2017, **56**, 11525-11529.
6. W.-C. Chen, B. Huang, S.-F. Ni, Y. Xiong, A. L. Rogach, Y. Wan, D. Shen, Y.Yuan, J.-X. Chen, M.-F. Lo, C. Cao, Z.-L. Zhu, Y. Wang, P. Wang, L.-S. Liao, C.-S. Lee, *Adv. Funct. Mater*., 2019, **29**, 1903112.
7. S. Kothavale, S. C. Kim, K. Cheong, S. Zeng, Y. Wang, J. Y. Lee, *Adv. Mater*., 2023, DOI: 10.1002/adma.202208602e2208602.
8. Z. Li, D. Yang, C. Han, B. Zhao, H. Wang, Y. Man, P. Ma, P. Chang, D. Ma and H. Xu, *Angew. Chem. Int. Ed*., 2021, **60**, 14846-14851.
9. T. Yang, B. Liang, Z. Cheng, C. Li, G. Lu, Y. Wang, *J. Phys. Chem. C*., **2019**, *123*, 18585-18592.
10. S. Wang, X. Yan, Z. Cheng, H. Zhang, Y. Liu, Y. Wang, *Angew. Chem. Int. Ed*., 2015, **54**, 13068-13072.
11. Y. Hu, Y. Yuan, Y.-L. Shi, D. Li, Z.-Q. Jiang, L.-S. Liao, *Adv. Funct. Mater*., 2018, **28**, 1802597.
12. R. Furue, K. Matsuo, Y. Ashikari, H. Ooka, N. Amanokura, T. Yasuda, *Adv. Opt. Mater*., 2018, **6**, 1701147.
13. J.-L. He, F.-C. Kong, B. Sun, X.-J. Wang, Q.-S. Tian, J. Fan, L.-S. Liao, *Chem. Eng. J*., 2021, **124**,130470.
14. H. Yu , X.-X. Song , N. Xie , J.-X. Wang , C.-L. Li and Y. Wang , *Adv. Funct. Mater.*, 2021, **31** , 2007511.
15. J.-L. He, Y. Tang, K. Zhang, Y. Zhao, Y.-C. Lin, C.-K. Hsu, C.-H. Chen, T.-L. Chiu, J. H. Lee, C.-K. Wang, C.-C. Wu, J. Fan, *Mater. Horiz*., 2022, **9**, 772-779.
16. S. Wang, Y. Miao, X. Yan, K. Ye, Y. Wang, *J. Mater. Chem. C*., 2018, ***6***, 6698-6704.
17. J. Xue, Q. Liang, R. Wang, J. Hou, W. Li, Q. Peng, Z. Shuai, J. Qiao, *Adv. Mater*., 2019, **31**, 1808242.
18. M. Zhao, M. Li, W. Li, S. Du, Z. Chen, M. Luo, Y. Qiu, X. Lu, S. Yang, Z. Wang, J. Zhang, S. J. Su, Z. Ge, *Angew. Chem. Int. Ed*., 2022, **61**, e202210687.
19. D. H. Kim, A. D'Aléo, X. K. Chen, A. D. S. Sandanayaka, D. Yao, L. Zhao, T. Komino, E. Zaborova, G. Canard, Y. Tsuchiya, E. Choi, J. W. Wu, F. Fages, J. L. Brédas, J. C. Ribierre, C. Adachi, *Nat. Photonics*., 2018, **12**, 98.
20. Y. Yu, H. Xing, D. Liu, M. Zhao, H. H.-Y. Sung, I. D. Williams, J. W. Y. Lam, G. Xie, Z. Zhao, B. Z. Tang, *Angew. Chem. Int. Ed*., 2022, **61**, e202204279.
21. U. Balijapalli, R. Nagata, N. Yamada, H. Nakanotani, M. Tanaka, A. D'Aléo, V. Placide, M. Mamada, Y. Tsuchiya and C. Adachi, *Angew. Chem., Int. Ed*., 2021, **60** , 8477.